Cold Regions Science and Technology 218 (2024) 104095

Contents lists available at ScienceDirect

Cold Regions Science and Technology

journal homepage: www.elsevier.com/locate/coldregions

An evaluation of ground-cooling systems in a saturated subarctic peatland

Ela Mastej [a,b,*], Stephanie Wright [a,c], Michael Braverman [d], Élise Devoie [c,e], Igor Egorov [f], William Quinton [a]

[a] Cold Regions Research Centre, Wilfrid Laurier University, 75 University Ave W, Waterloo, Ontario N2L 3C5, Canada
[b] School of Environmental Design and Rural Development, University of Guelph, 50 Stone Rd E, Guelph, Ontario N1G 2W1, Canada
[c] Department of Civil Engineering, Queen's University, 58 University Ave., Kingston, Ontario K7L 3N9, Canada
[d] GHD, 40 Bathurst Drive, Waterloo, Ontario N2V 1V6, Canada
[e] Department of Earth and Planetary Sciences, McGill University, 845 Rue Sherbrooke O, Montreal, Quebec H3A 0G4, Canada
[f] National Research Council Canada, 1200 Montreal Rd, Bld. M-20, Ottawa, Ontario K1A 0R6, Canada

ARTICLE INFO

Keywords:
Permafrost
Thermosiphon
Heat transfer
Snow reduction
Peatlands

ABSTRACT

The Canadian subarctic is one of the most rapidly warming regions on Earth. Permafrost thaw driven by climate change is linked to rapid landscape transition and is threatening northern infrastructure. Ground cooling systems are used in application-oriented projects largely pertaining to civil engineering operations and have been investigated in mineral-based soils with many successful outcomes. However, in near-saturated and peat-dominated environments they remain largely unexplored. The increasing rates of climate change and concomitant landscape evolution coupled with increasing economic activity in the North affirm the growing need for the advancement of ground cooling technologies in saturated peat-based soils. This study compared the performance of three ground cooling systems in saturated peat overlying thawing permafrost at the Scotty Creek Research Station in the Northwest Territories, Canada. The systems included a single-phase active thermosiphon combined with a snow reduction cone (advanced thermosiphon; ATS), a single-phase passive thermosiphon (simple thermosiphon; STS), and two stand-alone snow reduction cones. Performance was assessed based on subsurface temperature profiles (ranging 2017–2022), physical frost table measurements, and estimates of net annual and seasonal heat transfer. Each system displayed distinct ground cooling capabilities, successfully creating, and maintaining frozen ground. The ATS stood out with the highest net annual heat transfer rate, though it requires energy sources for actively circulating the coolant. The STS exhibited slightly lower effectiveness but demonstrated greater resilience to component failure. The snow reduction cone confirmed the significance of snow in ground insulation and augmented the performance of the thermosiphon system, enhancing its overall efficiency. It is anticipated that this study will foster the development of liquid-filled thermosyphons in the domain of cooling technologies, with a particular focus on their application in saturated peat and other similar environments. Moreover, these findings hold significant promise in offering valuable support for climate change adaptation strategies for local communities.

1. Introduction

The Dehcho region of the southern Northwest Territories (NWT), Canada is one of the most rapidly warming on Earth (Richter-Menge et al., 2017), and during recent decades, the rate of warming in the Dehcho is without precedent in the historical record (Vincent et al., 2015). Peatland-dominated terrain occupies approximately 35% of the discontinuous permafrost zones of the Taiga Plains, in which the Dehcho is located (Carpino et al., 2021). Here, permafrost is discontinuous and preferentially located in the peatland-dominated lowlands (Zoltai and Tarnocai, 1974). These lowlands are a mosaic of tree-covered peat plateaus overlying permafrost, juxtaposed with treeless, permafrost-free wetlands. The peat covering the ground surfaces of the plateaus is relatively dry and as such presents a highly effective thermal barrier that insulates the underlying permafrost (Camill, 1999). However, climate warming in the Dehcho has caused widespread permafrost thaw that is

* Corresponding author at: Cold Regions Research Centre, Wilfrid Laurier University, 75 University Ave W, Waterloo, Ontario N2L 3C5, Canada.
E-mail addresses: emastej@uoguelph.ca (E. Mastej), stephanie.wright@queensu.ca (S. Wright), Michael.Braverman@ghd.com (M. Braverman), elise.devoie@queensu.ca (É. Devoie), Igor.Egorov@nrc-cnrc.gc.ca (I. Egorov), wquinton@wlu.ca (W. Quinton).

https://doi.org/10.1016/j.coldregions.2023.104095
Received 18 November 2022; Received in revised form 12 December 2023; Accepted 13 December 2023
Available online 17 December 2023

transforming the land, (Carpino et al., 2021; Chasmer and Hopkinson, 2017) changing the distribution and routing of water (Connon et al., 2014; St. Jacques and Sauchyn, 2009), and damaging roads, air strips, ferry crossings, pipelines, buildings and other key infrastructure (GNWT, 2018), with resulting negative societal and economic consequences (Davidson et al., 2003). Permafrost thaw rates are greatest where climate warming is augmented by direct human disturbance of the ground surface (Raynolds et al., 2014). Disturbance invariably compresses the near surface peat layer, increasing its bulk density and moisture content that dramatically lowers the capacity of the surface layer to preserve permafrost (Williams et al., 2013).

It is widely acknowledged that permafrost thaw is transforming the Dehcho (Carpino et al., 2018; Haynes et al., 2019; Wright et al., 2022), driving an interest in the development of consumer-scale thaw mitigation strategies. Thermosiphons are the most widely used device for the prevention of permafrost thaw in diverse civil engineering contexts. Much research has been conducted on thermosiphon design, application, and optimization (Badache et al., 2019; Chen et al., 2018; Wagner, 2014; Xu and Goering, 2008) to improve the thermosiphon technology for a large-scale adaptation and mitigation applications. However, local, community and private-property applications of thermosiphon technology have not been explored and in this context cost efficiency and ease of installation become important considerations.

Thermosiphons are convective devices that extract heat from the ground and discharge it to the atmosphere (Long and Zarling, 2004). Originally, thermosiphons were designed as passive, sealed, pressurised pipes and were later modified to work as active and hybrid systems (Wagner, 2014). Thermosiphon technology has been developed in parallel in the US, Canada, China, and Russia, and has been used for permafrost cooling and foundation stabilization in the areas of continuous and discontinuous permafrost since 1960 (Richardson, 1979). The most notable thermosiphon installations were established along the Trans-Alaska Pipeline (completed in 1977) (Heuer, 1979; Wagner, 2014), in the Qinghai-Tibetan highway (Wu et al., 2010) and Qinghai-Tibetan railroad (Cheng et al., 2008) across the Qinghai-Tibetan Plateau; and Chaidaer-Muli railway in the southern part of the Qilian Mountains (Zhang et al., 2011). Applications of thermosiphons in road and rail embankments have been investigated extensively (for example, Forsstrom et al., 2002; Hayley et al., 1983; McFadden, 1985; Zhi et al., 2005; Xu and Goering, 2008; Zarling and Brayley, 1987). Other notable applications of thermosiphons include but are not limited to archaeological and culturally significant sites (Goetz, 2010) and containment and migration of contaminant transport from tailing (Edlund et al., 1998; Hayley et al., 2004). However, thermosiphons are applied almost exclusively to protect foundations and piles in large-scale, large-budget engineering projects, and extend into mineral sediments (e.g., Badache et al., 2019; Pei et al., 2019; Zhang et al., 2016), and as a result, there is relatively little information to guide thermosiphon design and application for shallow installation in wet organic terrains with discontinuous permafrost common throughout the Dehcho.

Commercially available thermosiphons are commonly “two-phase closed thermosiphons” (Azizi et al., 2013; Ahmed and Al Jubori, 2021; Brusly Solomon et al., 2017; Kim and Moon, 2021), and do not presently meet many of the needs in the Dehcho and other peatland-dominated regions with discontinuous permafrost throughout the circumpolar region (see Supplementary Material). For example, the cost of commercial thermosiphons is often prohibitively high and as such they are not a viable option for the growing number of potential users and applications. They also require heavy equipment (e.g., drilling rigs) for installation and the employment of certified engineers for their installation, all of which adds to their cost. Moreover, thermosiphon suppliers offer little or no option in terms of their basic design, leaving a wide array of other possible designs unavailable for purchase. This is in part due to the lack of research exploring different design possibilities and comparing their performance, particularly in saturated organic soils.

Developing a thermosiphon for a specific environment should consider the thermophysical conditions of the environment for which it is intended. In the Dehcho, the permafrost is relatively warm, being at or near the ice-nucleation temperature, relatively thin (<10 m), and discontinuous, occurring in distinct permafrost bodies of variable size (Quinton et al., 2009; Smith et al., 2010). As such, the permafrost in this region receives energy by vertical conduction from the overlying active layer and by horizontal conduction from adjacent, permafrost-free terrains, and thaw is easily initiated by small disturbances to the system including removal of canopy cover, increase in snow cover, increase in soil moisture among others (Devoie et al., 2021). These conditions stand in contrast to those at higher latitudes where permafrost is continuous, and much thicker and colder.

Consideration should also be given to the unique thermophysical properties of organic terrains and their effect on the preservation or thaw of permafrost. For example, the very high porosity (>85%) of the lightly decomposed peat near the ground surface enables an order of magnitude variation of its thermal conductivity with seasonal variations in its moisture content (Woo, 2012). As a result, the near-surface peat layer can seasonally alternate between functioning as an effective thermal conductor and an effective thermal insulator over relatively short periods (Pomeroy et al., 2007). Considering that this layer is the buffer between the ground and the atmosphere during summer, and the ground and snowpack during winter, its moisture content strongly affects the thermal condition of the underlying permafrost throughout the year (He et al., 2015). For the preservation of permafrost, the moisture content of the near-surface peat should be relatively low during summer so that the permafrost is insulated, but relatively high during winter so that the thermal energy accumulated in the permafrost during summer can be efficiently conducted away from it during winter (Brown, 1963). At greater depth in the supra-permafrost layer, where the peat is perennially saturated, the high porosity enables high volumetric moisture contents throughout the year, a condition that prolongs the duration of the zero-curtain periods during the fall (soil freezing) and spring (soil thawing) (Hayashi et al., 2007) compared with mineral soils which have much lower porosities and therefore lower maximum water contents.

The snow accumulation in the Dehcho is characteristically subarctic and as such is greater than at higher latitudes, and often exhibits considerable spatial variability due to variations in topography and/or vegetation (Faria et al., 2000). The thermal and optical properties of snow exert a primary influence on the winter heat loss from the ground. The temperature of the snow at the snow-atmosphere interface is relatively low due to its high albedo, emissivity, and exposure to wind (Cline, 1997; Marshall et al., 2003; Zhang et al., 2015). The very low thermal conductivity of cold, dry (i.e., non-melting) snow, due to high air content, restricts heat fluxes from the ground to the atmosphere (Cohen, 1994). As a result, permafrost tends to be warmer and more susceptible to thaw in areas of relatively deep snow (Jafarov et al., 2018). This common observation suggests that reducing the depth of snow, particularly in combination with thermosiphons, could enhance ground cooling or freezing (O’Neill and Burn, 2017).

To mitigate the insulative effects of snow accumulation, snow shades/sunshades (also referred to as snow sheds/sun sheds) have been used to reduce snow accumulation and cool winter surface temperatures while maintaining the surface temperatures during the summer at approximately the air temperature (Doré et al., 2016). The concept of a snow shading device serves a dual purpose of enhancing cooling in the winter and reducing heating in summer. By shedding snow, the device prevents snow accumulation on the ground in the winter, thereby eliminating the insulating effect of snow and allowing free circulation of cold air directly in contact with the ground underneath, consequently enhancing ground cooling. In the summer the device shades the ground from incoming solar radiation. The use of snow/sunshades have been applied to embankment protection in the areas of vulnerable permafrost. The technique was originally developed and tested in Alaska (Esch, 1988), and further tested along the Qinghai-Tibetan Railroad in China

(Wenjie et al., 2006; Niu et al., 2010) and on the Alaska Highway in Canada (Malenfant-Lepage et al., 2012a, 2012b). It has been demonstrated that temperatures at the surface of embankment slopes under snow/sunshades may be up to 6 °C lower on average when compared with unprotected slopes (Esch, 1988). Wenjie et al., 2006 reported a difference of 8 to 15 °C on the Qinghai-Tibetan Plateau (Wenjie et al., 2006), while Malenfant-Lepage et al. (2012a, 2012b) reported an annual heat flux of −10,000 kJ/m2 (cooling) for a snow/sunshade protected slope compared to +14,000 kJ/m2 (warming) for an unprotected slope (Malenfant-Lepage et al., 2012a). Although the snow/sunshades for embankment protection have not been widely adopted (Zarling and Braley, 1986; Doré et al., 2016), applying the concept of a snow shading cone with a thermosiphon could enhance its ground cooling performance, offering a promising solution for stabilizing permafrost in vulnerable areas.

This study evaluates the ability of a snow reduction cone and two different thermosiphon designs to freeze saturated peat under natural conditions. Peat is not only a widely occurring soil in the Dehcho and throughout much of the circumpolar subarctic but is also among the most challenging to cool and freeze given its high moisture content. As such, saturated peat environments are ideal for testing and improving ground-freezing designs. The performance of two passive systems were assessed: a snow reduction cone (hereafter "snow cone") and a relatively simple thermosiphon (STS) design. These systems are then compared with a more advanced thermosiphon (ATS) design that combines a snow reduction cone with an active cooling system intended to enhance its performance. We then assess the value of upgrading from a relatively simple/passive design to a more advanced/active thermosiphon design and make recommendations that consider factors, such as cost, ease of installation, and operation.

2. Study site

This study was conducted in the peatland-dominated zone of sporadic-discontinuous permafrost of the Northwest Territories (NWT), Canada, and the headwaters of Scotty Creek (61.18°N, 121.18°W), 60 km south of Fort Simpson (Fig. 1a). Scotty Creek is characterized by a subarctic climate with short dry summers and long cold winters. At Fort Simpson, mean annual air temperature (MAAT) is −2.6 °C (1981–2010), with January and July average values of −24.3 °C and 17.5 °C respectively (ECCC, 2021). During the study period (2018–2022), average summer (June to August), winter (November to April), and annual temperatures ranged from 14.3 °C to 17.6 °C, −20.5 °C to −15.4 °C, and − 3.5 °C to −1.9 °C, respectively. There was no significant trend in summer, winter, or annual temperatures over this period. Peat deposits at the study site range from 2 to 8 m in thickness and overlie a silty-clay to clay-rich glacial till (Connon et al., 2015; McClymont et al., 2013). The land cover is composed of peat plateaus that overlie permafrost and support black spruce forest, and treeless, permafrost-free wetlands including thermokarst bogs and channel fens (Fig. 1b; Zoltai and Tarnocai, 1974). Permafrost thickness ranges between 5 and 10 m (Burgess and Smith, 2000) and is isothermal at the ice nucleation temperature (Connon et al., 2018). Permafrost is therefore highly susceptible to various types of disturbance (e.g. vegetation removal, organic layer compression), where the depth to the permafrost table is approximately 0.7 m in undisturbed areas compared to >2 m below disturbed ground surfaces (Devoie et al., 2019). Detailed descriptions of the hydrological function and vegetation of each land cover type is provided by Quinton

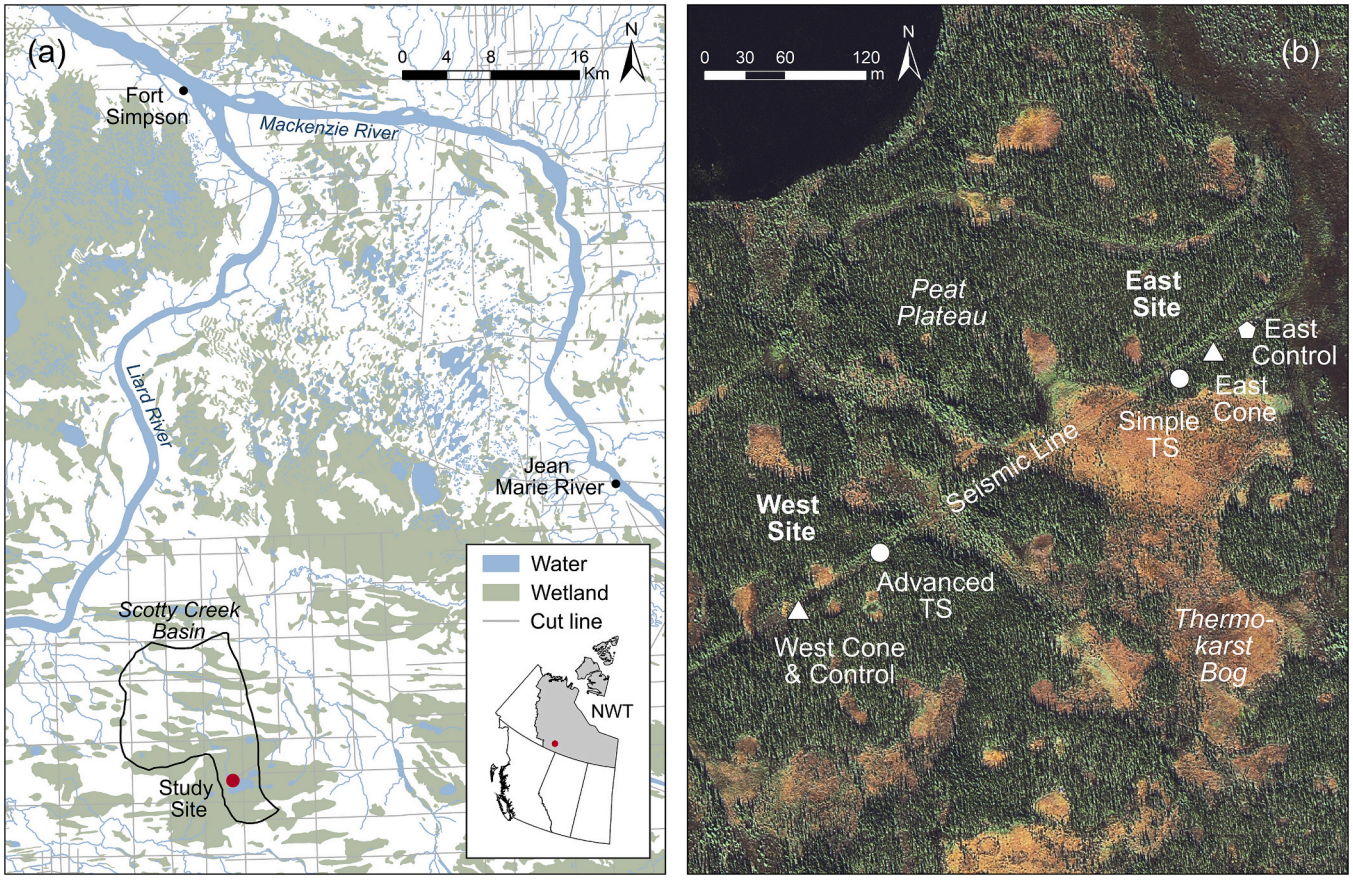

Fig. 1. (a) Location of study site relative to local communities and northwestern Canada (inset) and grid of seismic lines installed at Scotty Creek and surrounding areas in 1969. Map data sourced from Natural Resources Canada (2019). (b) Locations of ground cooling systems and controls along a seismic line installed in 1985 that intersects forested peat plateaus underlain by permafrost. Imagery from Worldview 3 captured in 2018.

et al. (2019) and Garon-Labrecque et al. (2015), respectively.

The most obvious and widely occurring anthropogenic impact on the land cover at Scotty Creek are seismic lines which are 6–10 m wide clearings used for oil and mineral exploration (Fig. 1; Williams et al., 2013). The first series of seismic lines at Scotty Creek were established in 1969, with a second series introduced in 1985. The density of seismic lines at Scotty Creek is 0.875 km km^{-2} (Quinton et al., 2011) which is about five times the natural drainage density of the basin. The present study was conducted along a 350 m section of a 1985 seismic line at points where the line traverses a peat plateau (Fig. 1b). The permafrost table below the seismic lines is relatively deep (> 1.5 m) compared to the adjacent undisturbed peat plateaus (~0.7 m).

3. Methods

The original intent behind the installation of thermosiphons was to investigate whether lost permafrost, resulting from surface disturbance (seismic lines) could be recovered. Two experimental sites were established in 2017 (Fig. 1b). The East Site is typically fully saturated at the end of the summer season with the water table at approximately ground surface level. In September 2017, permafrost was detected at 2.15 m below ground surface. The area was vegetated by a mixture of mosses (*Sphagnum* spp.), shrubs (*Rhododendron groenlandicum*), lichens (*Cladonia* spp.), and some sparse tree seedlings (*Picea mariana*). The West Site is located approximately 200 m from the East Site, on the elevated north side of the seismic line adjacent to the peat plateau. The permafrost table ranges from 1.37 m on the north side (measured August 2018) to 2.5 m toward the centre (measured September 2017). In late August 2018, a 0.70 m unsaturated zone was present, which is assumed to be the maximum depth to the water table. Vegetation was of the same composition as the East Site but with a higher proportion of lichens (*Cladonia* spp.). The instrumentation at each site consists of a ground control, snow cone, and thermosiphon (TS). Each system and site-specific conditions are further described below.

3.1. Control sites

The West Control site was established in September 2017 on the peat plateau at the south side of the seismic line (Fig. 1b). A profile of six Campbell Scientific model 109 (CS109) thermistors (±0.1 °C) were installed in the soil to a depth of 2.5 m, which was approximately the depth of the permafrost table at the time of installation (Fig. 2a). The East Control site was also established in September 2017 with a profile of five CS109 thermistors installed to the top of permafrost at a depth of 2.15 m (Fig. 2b). Campbell Scientific CR800 and CR200 data loggers recorded average temperatures every 30 min at the West and East Control sites, respectively. Values were then averaged to daily intervals for analysis.

3.2. Snow reduction cone

Two snow reduction cones were constructed at the East and West Sites to evaluate the ground thermal response to a reduction in the depth of the overlying snow cover. The thermal impact of a snow cone was evaluated separately from the thermosiphons to determine its effectiveness as a stand-alone system and for integration into the design of the advanced thermosiphon. The East Cone was installed in the centre of the seismic line ~30 m west of the East Control and the West Cone was installed at the south edge of the seismic line approximately 1.0 m from the West Control. No permafrost was detected with a 1.5 m probe at the end of August 2018 under and around the snow cones.

Each snow cone was made by cutting a galvanized steel sheet, which was then attached to an aluminum frame tripod. The cone diameter and height were 1.0 m and 0.6 m, respectively. The top of each cone had a

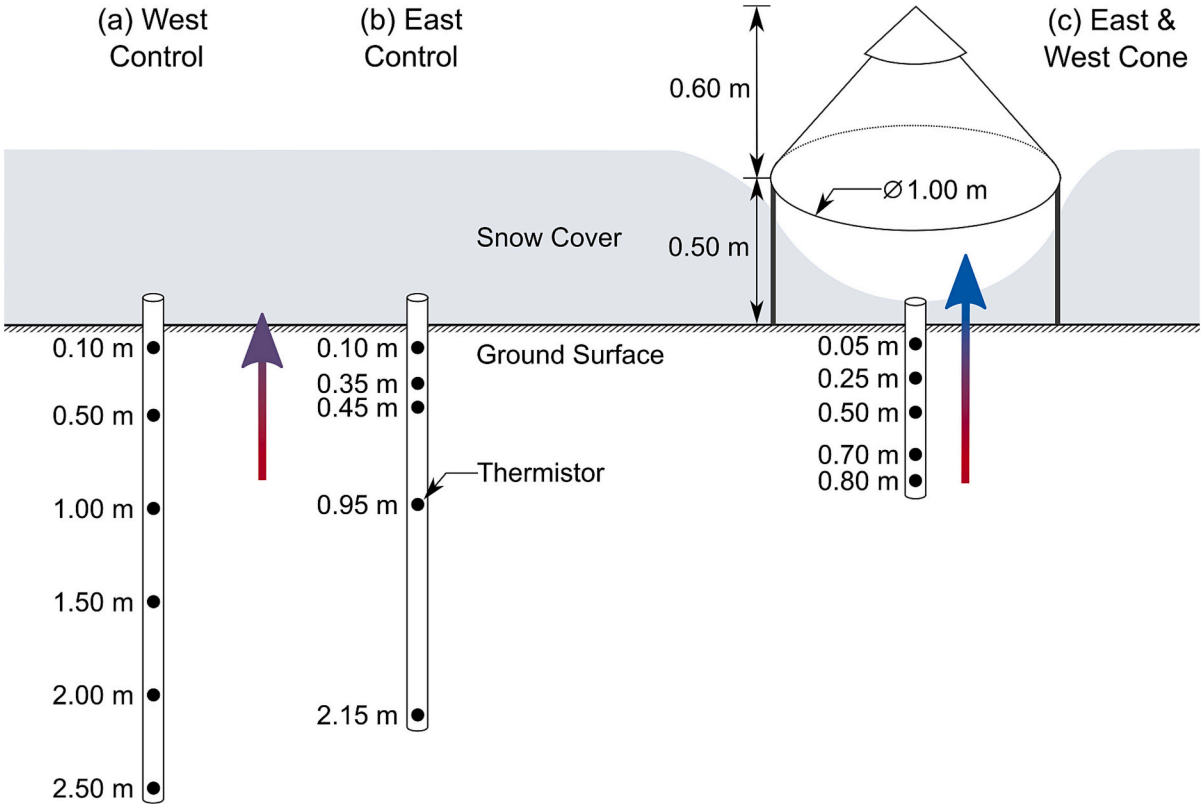

Fig. 2. Thermistor depths for the west (a) and east (b) control systems. (c) Snow deflection cone design and thermistor depths for the East and West Cones. Shaded red to blue arrows indicate the direction of heat transfer with the nearby ground and air in winter. (For interpretation of the references to colour in this figure legend, the reader is referred to the web version of this article.)

10 cm opening to allow air circulation and a smaller cone with a 0.25 m diameter was attached above it on a round steel frame to prevent snow accumulation under the cone through the top opening (Fig. 2c). The average distance between the ground and the cone base was approximately 0.50 m. Thermistors (CS109) were installed directly below the centre of the cone to a depth of 0.8 m. A Campbell Scientific CR200 data logger recorded average temperatures every 30 min, then averaged to daily intervals for analysis.

3.3. Simple thermosiphon

A relatively simple thermosiphon was installed in the seismic line ~10 m from the north edge of the plateau and ~ 30 m from the East Control (Fig. 1b). It was installed in February 2019 and deactivated in June 2020. The STS design was single phase and passive, consisting of a larger-diameter outer pipe (aluminum), and a smaller inner pipe (PVC) sharing a common axis (coaxial) and extending to the same depth (Fig. 3a). The internal pipe was open-ended at the top and included 5 cm long parallel slots at the bottom. A GeoPrecision TNode thermistor string (±0.1 °C) was attached outside of the exterior pipe extending to 1.5 m depth (Fig. 3a). Temperatures were recorded hourly and averaged to daily intervals for analysis.

In a passive system the internal working fluid (glycol-based commercial antifreeze in this case) circulates by natural convection generated from differences in temperature (and therefore density) of the coolant (Rahman and Saghir, 2014), and radiative heat transfer to the atmosphere. When air temperatures fall below that of the coolant in the above-ground portion of the pipe, the latter cools, densifies, and sinks downward through the space between the inner and outer pipe. At the bottom of the pipe, the coolant is warmed by the ground at that depth and its density decreases, causing it to flow through the perforations and rise through the inner pipe. The inner pipe therefore separates the rising and sinking liquids and facilitates circulation while decreasing turbulent mixing. Once the air temperature rises above the ground temperature, convection within the device stops.

3.4. Advanced thermosiphon

An advanced thermosiphon system (Fig. 3b) was established in August 2018, located approximately 50 m from the West Control and snow cone (Fig. 1b). The advanced design was also single phase, but circulation of the fluid was mechanically driven (i.e., active) rather than driven by density differences alone (i.e., passive). The ATS design included a mechanical pump affixed to the top of the pipe which used a simple thermostat to activate the pump only when the air temperature was below 0 °C. The ATS consisted of a 3 m long aluminum pipe with interior and exterior diameters of 8.2 cm and 8.9 cm respectively, which was filled with the same liquid coolant used in the STS (Fig. 3b). A snow cone was mounted to the exterior wall of the pipe so that the base of the cone was 0.5 m above the ground surface (Fig. 4a). The pipe was inserted to a depth of 1.37 m below ground surface, which was the maximum thaw depth at the time of installation. Thermistors (CS109) were attached to the outside of the exterior pipe, extending to 1.4 m depth (Fig. 3b). A Campbell Scientific CR300 data logger recorded average temperatures every 30 min and then averaged to daily intervals for analysis. A GeoPrecision TNode thermistor string (±0.1 °C) was installed 0.25 m from the wall of the thermosiphon under the cone and recorded average temperatures every 15 min. The intent of the

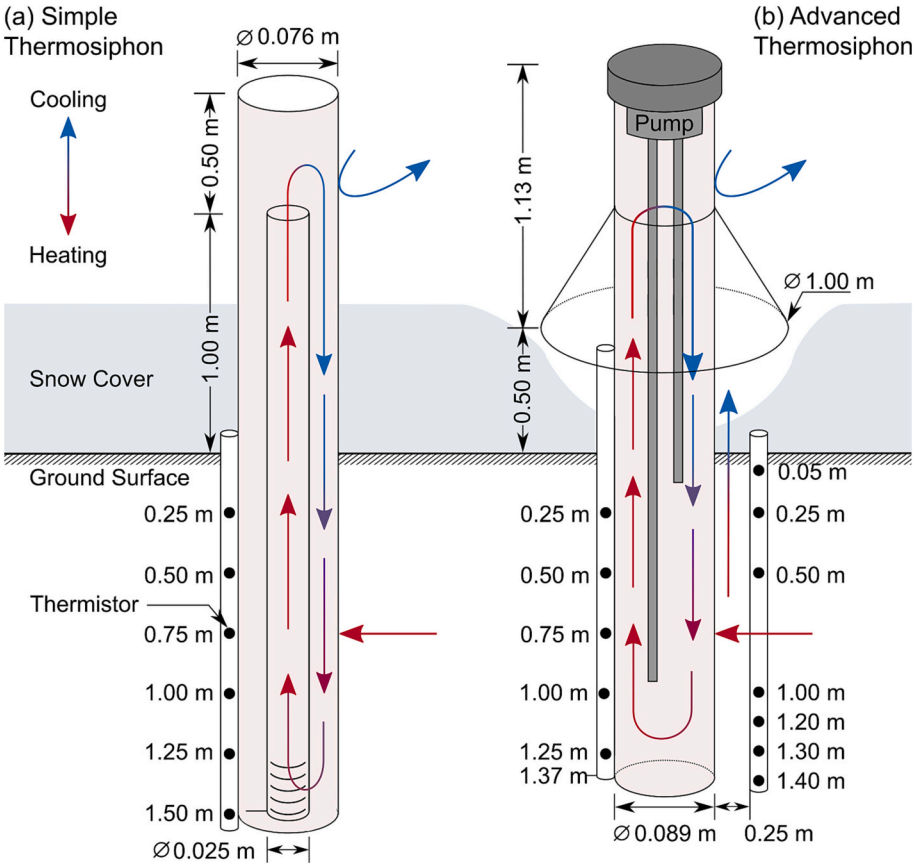

Fig. 3. (a) Simple and (b) advanced thermosiphon designs and thermistor depths. Red and blue arrows indicate the direction of heat transfer with the nearby ground and air in winter. The working fluid sits near the top of the thermosiphon in summer but lowers in winter due to thermal contraction. It is important to consider the coefficient of thermal expansion of the fluid, ensuring that the internal pipe always remains submerged for proper operation. (For interpretation of the references to colour in this figure legend, the reader is referred to the web version of this article.)

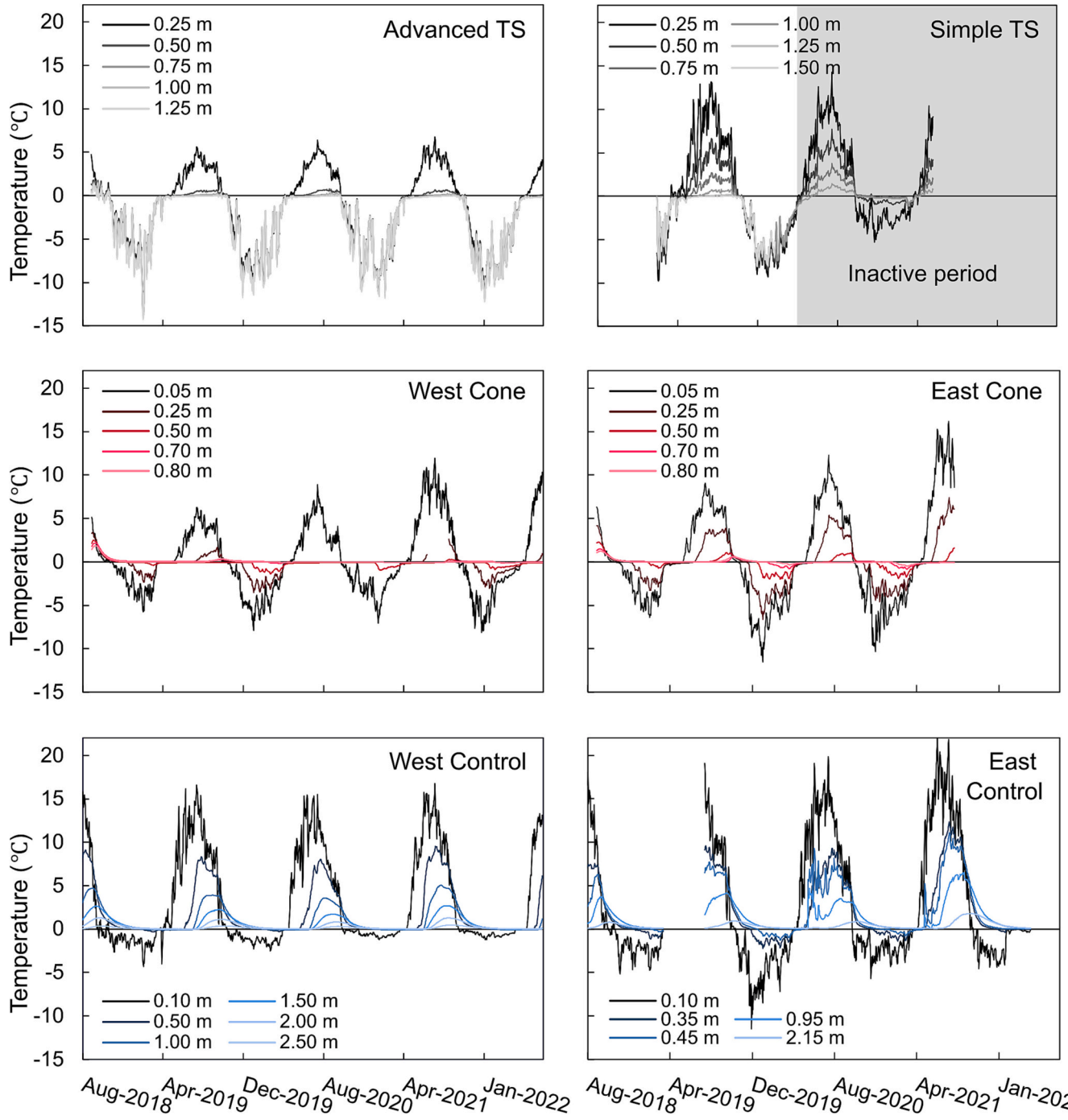

Fig. 4. Average daily ground temperature measurements for each ground cooling system and control where line colours are brighter as measurements increase in depth. Ground temperatures for the Active TS and Simple TS were measured along the TS wall. The Simple TS was deactivated early June 2020.

installation was to place the base of both thermosiphons at the depth of maximum thaw. Although either installation did not extend into the permafrost, both extended beyond the active layers traversing the taliks, with the aim of refreezing them. The elimination of a talik is a necessary step for permafrost aggradation. The rationale behind this methodology is that this would be the recommended procedure for small-scale, community and private property installation.

3.5. Heat transfer analysis

3.5.1. Snow reduction cones

The dominant heat transfer mechanism for the controls and snow cones is vertical conduction to and from the ground surface (red arrows in Fig. 2). To estimate vertical flux, each soil profile was divided into several homogenous horizontal layers based on thermistor depths. The thermal conductivity was estimated for each layer at a daily time step using Eq. (1):

$$K_{d,s,f} = K_{a,l,i}(\eta) + K_{peat}(1-\eta) \quad (1)$$

where $K_{d,s,f}$ [W/m°C] is the bulk thermal conductivity for a dry unfrozen/frozen (K_d), saturated unfrozen (K_s), or saturated frozen (K_f) soil layer. $K_{a,l,i}$ [W/m°C] is the thermal conductivity of air ($K_a = 0.025$ W/m°C), liquid water ($K_l = 0.6$ W/m°C), or ice ($K_i = 2.14$ W/m°C), K_{peat} is the thermal conductivity of peat (0.25 W/m°C), and η [−] is the porosity

of the soil (Woo, 2012). A soil layer was assumed frozen if its temperature fell below 0 °C since the freezing-point depression (−0.01 °C to −0.07 °C) estimated from the ground temperature data fell within the accuracy range of the thermistors (±0.1 °C). To account for the uncertainty in the porosity of peat, a minimum, average, and maximum value was used to calculate $K_{d,s,f}$ for each soil layer (table in Supplemental Material) using Scotty Creek measurements by Quinton et al. (2008). A bulk thermal conductivity for the profile was calculated using the depth-weighted harmonic mean of all soil layers to a maximum depth of 1 m. This value was then used with Fourier's law to compute daily heat flux [W/m^2], where the thermal gradient was calculated using ground temperatures at or near 0.25 m below ground surface and at or near 1 m for each system (Lienhard IV and Lienhard V, 2006) which are the most consistent depths across systems. The resulting flux was multiplied by the area under a cone (0.79 m^2) for all systems and summed for each year to compare daily and net annual heat transfer [in W] for the near surface 0.8–1.0 m.

For all systems at the East Site, the ground was assumed to be fully saturated all year based on visual observations of the site. For the West Site systems, an average unsaturated zone of 0.50 m was assumed for all of August and September with no unsaturated zone (i.e., fully saturated) for the remainder of the year. This assumption is based on data patterns from a water level recorder near the site. In the absence of continuous moisture content values, these assumptions are aligned with previous knowledge of the site and are considered conservative.

3.5.2. Thermosiphons

The predominant mechanism for radial heat transfer to and from the ATS and STS is conduction (red horizontal arrow in Fig. 3). To calculate the radial heat transfer, the system was again divided into uniform horizontal layers that consist of the same porosity and saturation conditions for the east and West Sites as used for the vertical heat transfer calculations. The freeze/thaw radius surrounding the thermosiphon was then computed for each soil layer using a closed-form solution to the heat equation with phase change in cylindrical coordinates from Jaeger and Carslaw (1959):

$$2R^2 ln\left(\frac{R}{a}\right) - R^2 + a^2 = 4\frac{K_{d,s,f}Tt}{\eta L} \quad (2)$$

where R [m] is the radius of the freezing or thawing front spreading from the thermosiphon, a [m] is the outer radius of the thermosiphon (ATS = 0.045 m, STS = 0.038 m), $K_{d,s,f}$ [W/m°C] is the bulk thermal conductivity of the soil (computed from Eq. (1)) up to radius R, T [°C] is the temperature of the thermosiphon, t [s] is time since freeze/thaw initiation, and L [J/kg] is the latent heat of fusion of water (334,000 J/kg).

To calculate the thermal gradient, it was assumed that the ground temperature outside of the radius of freezing was equal to the ground temperatures measured at the control sites, and the temperature at the freezing/thawing front was at the freezing point (0 °C). Assuming an equilibrium temperature gradient between the thermosiphon and freezing front, R was used with the control data to apply Eq. (2) to calculate the heat flux at a daily time step for each soil layer along the thermosiphon and summed using the thermosiphon area to obtain the total radial heat transfer. Details of soil properties in each layer are included in Table 1. In the case of changing from freezing to thawing (or vice-versa), the freezing or thawing duration, t, is reset. This allows to change between thawing and freezing seasonally. However, in shoulder seasons there are often short duration events (e.g., three above-zero days in early winter). To maintain all the previous freezing information (e.g., from the early winter), the previous maximum freeze/thaw radius, R, and the time, t, is stored to compare to the new position of the freeze/thaw interface. This allows the solver to recover from short-duration warm or cold spells without significant information loss.

Once the radius of freeze/thaw is established using Eq. (2) the radial heat flux to or from the thermosiphon can be calculated assuming a linear temperature gradient between the temperature measured at the wall of the thermosiphon and the freezing point, a distance R from the thermosiphon. It is assumed that the radial temperature distribution is steady state (i.e., linear). Due to the slow nature of temperatures fluctuations, it is likely that this assumption is realistic. The thermal conductivity is chosen to reflect the frozen/thawed state of the soil. This calculation is repeated to calculate the thermal flux for each thermistor depth and summed using the thermosiphon area to obtain the total radial heat transfer. Given the equilibrium assumptions, this is a conservative estimate of radial heat transfer. Vertical heat transfer was also calculated for the thermosiphons as described in Section 3.5.1 and added to the radial value to estimate total heat transfer for each thermosiphon.

4. Results

4.1. Control sites

Ground temperature time series for the West Control are generally consistent for each winter and summer between 2018 and 2022 (Fig. 4). At the end of August 2018 (when the ATS and snow cones were installed) the ground temperatures at the West Control site, at 0.5 m, 1.0 m, and 1.5 m below the ground surface, were 7.7 °C, 4.7 °C and 2.4 °C respectively. Ground temperature time series for the East Control have generally consistent patterns between 2018 and 2021 summers, but winter ground temperatures are more variable with the lowest occurring in winter 2020 (Fig. 4).

Maximum and minimum ground temperatures are generally greater at the East Control compared to the West Control, particularly near surface (Fig. 5). For example, maximum and minimum ground temperatures in 2021 at 0.1 m were 16.78 °C and − 1.18 °C for the West Control, compared to 22.40 °C and − 4.58 °C for the East Control. However, average winter and summer ground temperatures between 0.5 and 1.5 m (selected depth for consistency) for 2018–2021 are comparable at both control sites (Table 2), which can be expected considering lower ground temperature fluctuations at increasing depths. Average winter ground temperatures typically hover around the freezing point for both sites.

Table 1
Range of porosity values used in heat flux calculations for each soil depth and corresponding frozen/unfrozen thermal conductivity.

	Soil Depth (m)	Porosity, η			Thermal Conductivity (W/m°C)					
		Avg.	Max.	Min.	Avg. Frozen	Avg. Unfrozen	Max Frozen	Max Unfrozen	Min Frozen	Min Unfrozen
Unsaturated	0.05–0.10	0.94	0.97	0.91	0.04	0.04	0.03	0.03	0.05	0.05
	0.25–0.35	0.86	0.93	0.79	0.06	0.06	0.04	0.04	0.07	0.07
	0.40–0.50	0.83	0.88	0.78	0.06	0.06	0.05	0.05	0.07	0.07
Saturated	0.05–0.10	0.94	0.97	0.91	2.03	0.58	2.09	0.59	1.96	0.94
	0.25–0.35	0.86	0.93	0.79	1.88	0.55	2.01	0.58	1.74	0.53
	> 0.40	0.83	0.88	0.78	1.82	0.54	1.92	0.56	1.72	0.52

Values are from Quinton et al. (2008) using Eq. (1) and component (i.e., water, ice, air, peat) thermal conductivities in Section 3.5.1.

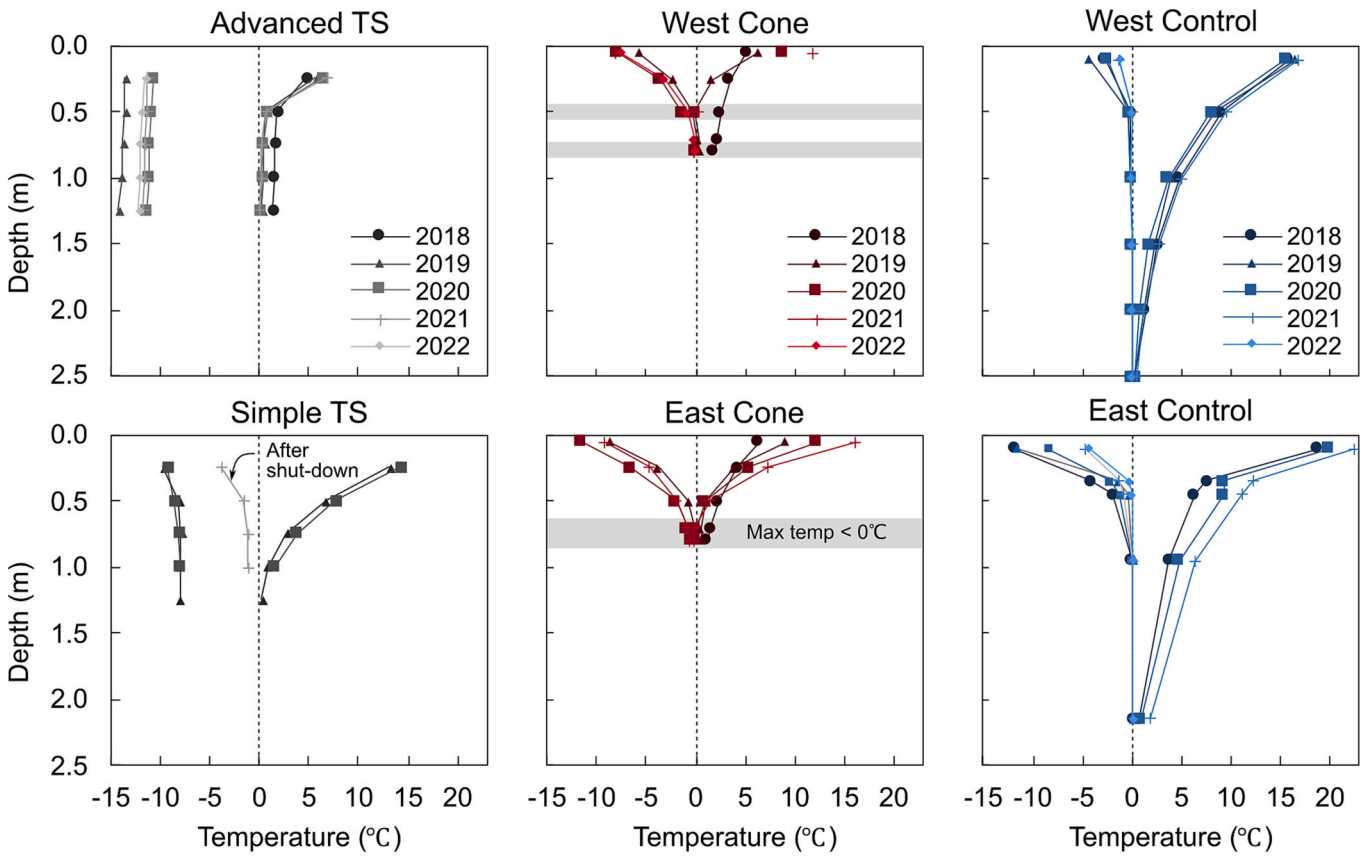

Fig. 5. Annual ground temperature envelopes for each system based on measured maximum and minimum average daily ground temperatures. The shaded grey bar indicates depths where maximum ground temperatures were reduced below 0 °C for at least one year. Note, maximum and minimum ground temperatures are not available for all years at all depths due to malfunctioning sensors or power issues.

Table 2
Average winter (measured for Feb–Apr) and summer (measured for May–Aug) ground temperatures in °C between depths of 0.5–1.5 m.

	Average Winter Temperature (°C)			Average Summer Temperature (°C)		
	2019	2020	2021	2019	2020	2021
West Control	−0.06 ± 0.04	−0.04 ± 0.05		1.5 ± 2.5	1.5 ± 2.4	2.2 ± 3.0
Advanced TS	−3.9 ± 3.8	−5.7 ± 2.7	−6.1 ± 2.9	0.9 ± 1.6	0.9 ± 1.8	
East Control		−0.06 ± 0.3	0.01 ± 0.2		2.1 ± 1.9	2.6 ± 2.8
Simple TS	−2.1 ± 2.1	−3.5 ± 2.1		1.0 ± 1.6		

This depth range was selected for consistent comparison between thermistor profiles. Standard deviation is represented by ±.

4.2. Snow reduction cone

During the winter of 2018/2019 snow accumulation around the snow reduction cones gradually reduced the snow-free area at the base of the cones. However, at the peak of snow accumulation around the cones, there was a visible snow-free area at the base of the cones approximately 4 cm wide and 60 cm long at the East Cone (no data available for the West Cone), which allowed for the air circulation and consequent heat loss from the ground to the atmosphere. Images from an infrared camera (Flir, E5XT) also measured higher temperatures under the East Cone than surrounding snow-covered areas, indicating increased heat removal from the ground (Fig. A1 in Supplementary Material).

Ground temperature time series for the East Cone show distinctive and consistent results for all three winter seasons (Fig. 4). Similar to the control sites, ground temperature ranges were larger for the East Cone than the West Cone (Fig. 5). Average temperature between 0.7 and 0.8 m below ground surface was selected as a critical depth in the active layer for the comparison of the snow cones and controls. For the East Cone, the average temperatures within the soil vertical profile between 0.70 and 0.80 m below the ground surface were consistent for all three winters between 2019 and 2021 (Table 3). Notably, average summer ground temperatures at these depths were similar to winter. The winter ground temperatures were comparable to the East Control site, measured at 0.75 m. However, summer ground temperatures at the East Control site were considerably higher ranging between 2.8 and 3.3 °C and showed an increasing trend. The West Cone also showed similar average annual ground temperature trends for both winter and summer seasons. Average summer and winter ground temperatures for both cones were comparable. Similar to the East Cone, average summer ground temperatures for the West Cone were lower than at the West Control site at 0.80 m below the ground surface (large data gap for 0.70 m), which ranged between 2.1 °C and 3.3 °C.

At the end of August 2019 there was a 0.15 m thick frozen layer around both cones at a depth between 0.60 and 0.75 m below the ground surface. The radial distance of the frozen ground was approximately 0.50 m from the edge of the cones. The frozen lens was maintained during the summers of 2020 and 2021 under the East Cone as evidenced by the consistent below 0 °C temperatures at the ground depths between 0.70 and 0.80 m (Figs. 5 and 6b). Under the West Cone, below 0 °C temperatures were maintained at 0.50 m in 2019 and 2020, and at 0.80 m in 2020 and 2021. The thermistor at 0.70 m malfunctioned between May 2020 and September 2021, but frost probing suggests this depth

Table 3
Average winter (measured for Feb-Apr) and summer (measured for May-Aug) ground temperatures in °C at the 0.7–0.8 m soil profile for the East Cone, 0.8 m for the West Cone, and 0.75 m for east and west control sites. Standard deviation is represented by ±.

	Average Winter Temperature (°C)			Average Summer Temperature (°C)		
	2019	2020	2021	2019	2020	2021
West Control	−0.1 ± 0.04	−0.08 ± 0.06	−0.05 ± 0.01	2.1 ± 2.4	2.1 ± 2.3	3.0 ± 3.0
West Cone	−0.02 ± 0.002	−0.03 ± 0.009	−0.07 ± 0.02	−0.01 ± 0.02	−0.04 ± 0.003	−0.05 ± 0.006
East Control		−0.2 ± 0.1	−0.07 ± 0.1		2.8 ± 1.8	3.3 ± 2.9
East Cone	−0.02 ± 0.005	−0.3 ± 0.2	−0.4 ± 0.2	−0.02 ± 0.004	−0.1 ± 0.02	−0.1 ± 0.03

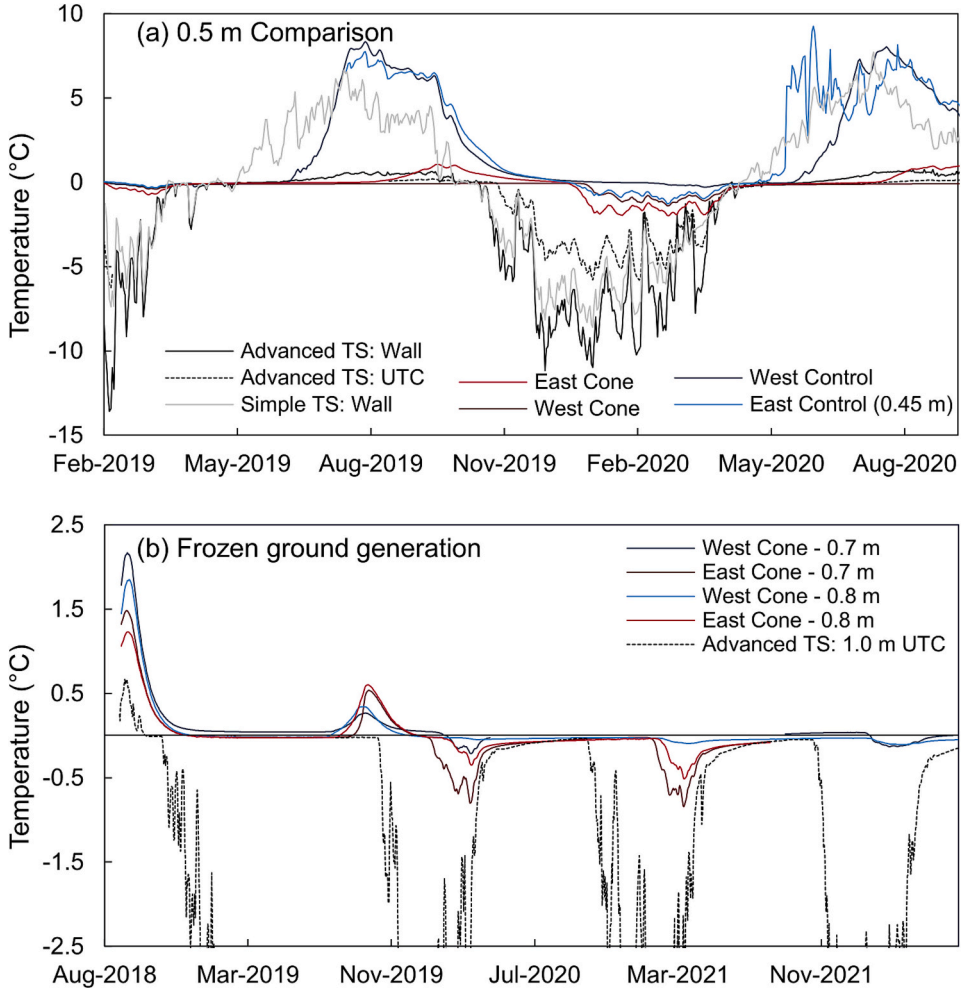

Fig. 6. (a) Comparison of daily average ground temperatures at 0.5 m depth for all systems and controls except for the East Control where ground temperatures are from 0.45 m. (b) Daily average ground temperatures for depths where frozen ground was generated (i.e., temperatures remained below 0 °C). Note that the vertical scale has been magnified and UTC = under the cone and TS = Thermosiphon.

likely also remained frozen. By September 2022, the frozen lens grew to 0.29 m thick between 0.61 and 0.9 m under the West Cone and 0.49 m thick between 0.66 and 1.15 m under the East Cone. In each of these cases, the enhanced heat export due to the lack of snow cover under the cone resulted in the formation and growth of permafrost in the previously permafrost-free sites, extending beyond the direct footprint of the snow cone itself. This radial freezing beyond the cone can be explained through radial heat transfer, where the cooling induced by the snow cone affects a surrounding region through radial conduction. No permafrost was detected beneath these generated frozen layers of each cone with a 2.0 m frost probe.

4.3. Simple thermosiphon

The STS design explored the efficacy of the natural convective heat transfer and the capacity of this model to maintain low ground temperatures within the active layer. Prior to the installation at the beginning of February 2019, the initial ground temperatures for all three depths of 0.5 m, 1.0 m and 1.5 m below the ground surface were −0.1 °C. Winter-time ground temperatures between 0.5 and 1.5 m were very similar indicating the thermosiphon was functioning correctly and heat transfer was occurring along the thermosiphon pipe (Fig. 4). Five days after the installation the average ground temperature at these depths was −7.2 °C (±0.2), whereas at the East Control site it was 0.10 °C (±0.05). The average ground temperature between 0.50 and 1.50 m was considerably lower than the East Control site during the

winter and moderately lower in the summer (Table 2). Maximum ground temperatures did not remain below freezing during summer (Fig. 5). This observation suggests that heat transfer through conduction likely played a significant role, facilitated by both the internal fluid within the thermosyphon and the pipe that constitutes the thermosyphon itself. A similar process could have influenced the cold bias during winter. Summer ground temperatures at 0.5 m were similar to the control, but onset of spring thaw occurred a few weeks earlier (Fig. 6a). Following the deactivation of the thermosiphon, winter ground temperatures more closely reflected the ground temperatures at the East Control, indicating the effectiveness of the STS at cooling the ground while operational (Fig. 5).

4.4. Advanced thermosiphon

The ATS design aimed to investigate the combined impact of forced convection (achieved through a pump-enhanced movement of heat-carrying liquid) and the absence of snow insulation on ground cooling. The study observed ground temperature patterns at different depths from the onset of consistent below 0 °C temperatures within the soil profile in late October 2018 until mid-April 2019. The results demonstrated a consistent heat transfer along the thermosiphon pipe (Fig. 4). During the first winter after installation, a period of battery failure led to the pump shutting down in December 2018 and January 2019. Additionally, the snow cone failed to maintain a snow-free area, resulting in thorough insulation of the ground surface under the cone by the end of December 2018. Despite the pump shutdown in December, there was a decreasing ground temperature trend due to the combined effects of natural convective heat transfer within the thermosiphon and ground heat loss through the snow-free surface. In January, as snow gradually covered the ground, the rate of vertical heat transfer was impeded. At the beginning of February 2019, the snow around the cone (approximately 0.70 m in depth) was removed, and the pump was reactivated. Within two days, ground temperatures along the thermosiphon wall reached their minimum seasonal values, ranging from −13.3 °C to −14.2 °C. These findings underscore the importance of considering snow and pumping efficiency in ground cooling systems and offer valuable insights for future installations. Comparing the ATS profile with the STS, it was observed that maximum and minimum annual temperatures were generally lower for the ATS (Fig. 5). Notably, winter ground temperatures measured at 0.5 m were similar between both TS systems (Fig. 6a). However, the average winter and summer ground temperatures between 0.5 and 1.5 m were lower for the ATS compared to the West Control and the STS. Furthermore, there was a decrease in average winter ground temperatures between 2019 and 2021 (Table 2). By the end of August 2019, perennial frozen ground was observed around the thermosiphon/cone system at 0.70 m depth, extending 55–90 cm radially from the cone edge. By early September 2022, a frozen “half egg shape” was present around the cone edge at an average depth of 0.59 m, extending radially 0.50–1.00 m toward the center of the seismic line (southwest) and over 200 cm toward the undisturbed plateau (northeast).

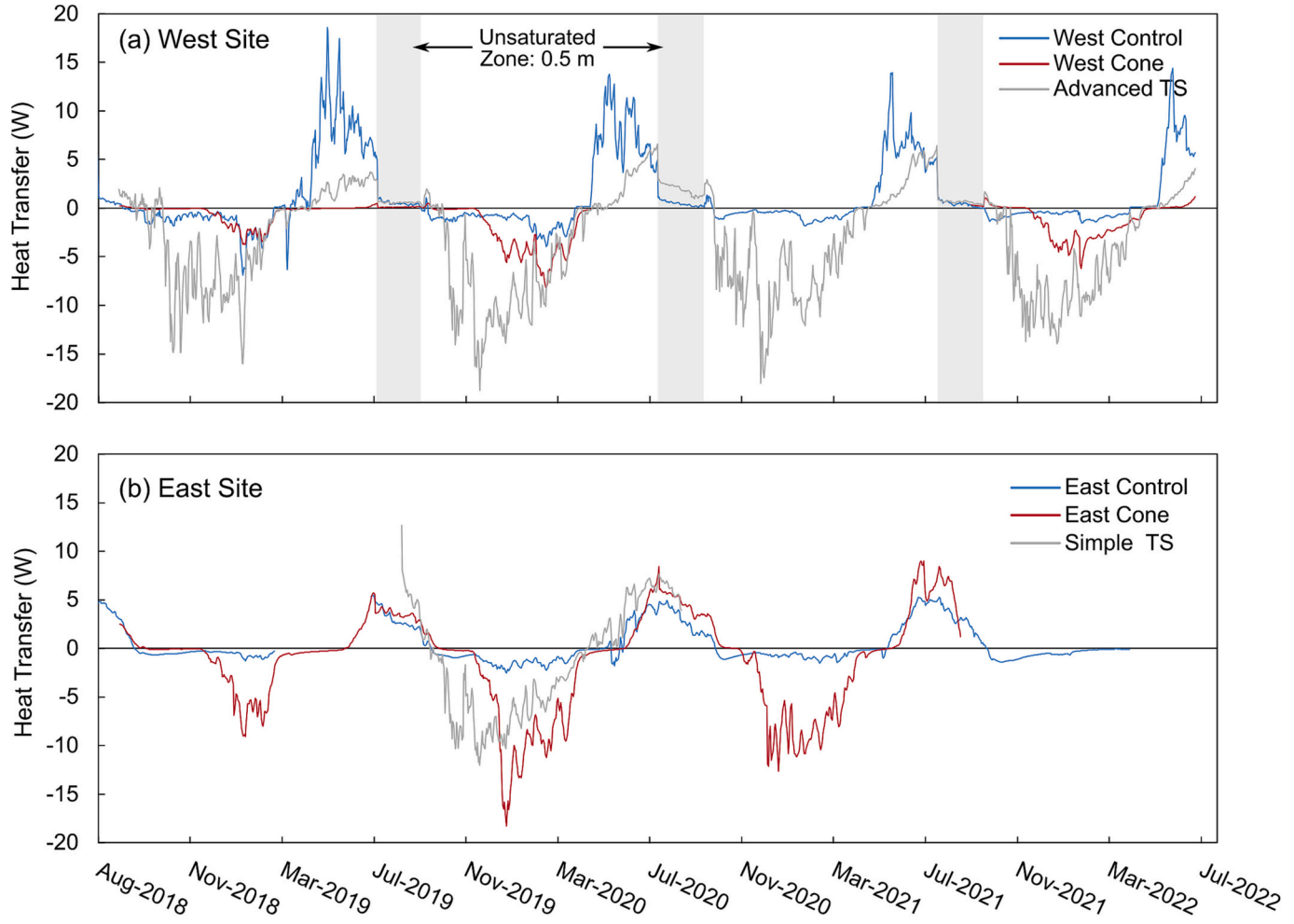

Fig. 7. Summary of daily heat transfer estimated for each system at the (a) West Site and (b) East Site. Calculations for the East systems assumed saturated conditions year-round, whereas the West Site assumes a 0.5 m unsaturated zone from August 1 to September 30 of each year.

4.5. Heat transfer

Daily heat transfer was calculated for each ground cooling system and control, where each system at the West Site had a 0.50 m unsaturated zone for August and September and the East Site remained fully saturated year-round (Fig. 7). The introduction of an unsaturated zone dramatically reduced the heat transfer for all systems and controls. For the West Control, ground heat loss during the winter (negative heat transfer) was smallest in magnitude compared to the West Cone and ATS, and heat gain (positive heat transfer) was the greatest. This resulted in a net annual warming of the West Control site for all three years of analysis (Table 4). The West Cone promoted earlier (6–8 weeks) and greater heat loss in winter relative to the control due to enhanced snow reduction. Summer heat gains were also delayed (4–6 weeks) and reduced compared to the control. Overall, the West Cone lost heat for each year of analysis with greater heat loss occurring in 2019–2020. The ATS produced the earliest and greatest heat loss over winter and the lowest heat gain in summer, resulting in an order of magnitude more heat loss annually compared to the West Cone (Table 4).

The heat transfer patterns for the East Site are similar to the West Site for the years where all systems are active (Fig. 7). The main difference between the two sites was that the heat gain in summer was similar between all the east systems and occurred with minimal lag times, while there were clear differences in summer heat transfer between the west site systems. Heat transfer for the East Cone in the summer was also higher than the East Control, but this was offset by the much greater heat loss in the winter resulting in net ground cooling. Net annual heat transfer was more variable for the East Cone and control from year-to-year. This may be due to saturated conditions resulting in a closer thermal coupling between ground and air temperatures (due to higher thermal conductivity) leading to greater interannual variability.

When comparing the seasonal heat transfer across systems at both sites, the advantage of a thermosiphon is clear as it starts to cool the ground in early fall (Table 5). During winter at the West Site, similar results as the net heat transfer estimates can be seen where the ATS removes the most heat followed by the snow cone. Interestingly, this is not the case at the East Site where the snow cone appears to remove more heat than the STS. This may be attributed to site specific heterogeneity or indicate that the cone excels when the ground is highly saturated. Although it was expected that the snow cone would also provide cooling through summer shading, the heat transfer in summer is relatively comparable across all sites and systems.

5. Discussion

5.1. Thermosiphon comparison

Both thermosiphon designs enhanced the rate of heat removal from the ground relative to the control sites. Moreover, both sites instrumented with thermosiphons demonstrated an annual net negative energy balance as manifested by ground cooling, while the ground below the control sites warmed over the same period (Tables 3 and 4). The STS and ATS designs performed similarly at 0.5 m below the ground surface as demonstrated by the converging ground temperature profiles (Fig. 6a). However, at the 1.0 m and 1.5 m depths, the ATS removed more heat from the ground. The cooling rate as indicated by the time lag between a change in air temperature and the subsequent change in ground temperature was not significantly different between the two designs (Fig. 6a). However, the ground surrounding the ATS cooled to lower temperatures, and the net annual heat transfer for 2019–2020 at that site was 2.6 times greater than that at the STS site. Although the ATS performed considerably better from an annual energy budget perspective, the seasonal comparison suggests the ATS is not considerably more effective than the STS when operating in winter (Table 5). It is important to note that the East site where the STS is located is wetter than the ATS which would enhance the total heat transfer once frozen. The ATS generated and maintained frozen ground throughout the year (Fig. 6b), which is attributed to the enhanced circulation provided by the pump and enhanced cooling provided by the cone in winter and summer.

Although the STS did not maintain ground temperatures below 0 °C throughout its year of operation, the net negative heat transfer calculated for this design suggests it could generate frozen ground with continued operation. The initial presence of permafrost determines the trajectory of below 0 °C ground temperatures, so the difference in initial depth to permafrost between the ATS and STS likely influenced the results. Annual below 0 °C ground temperatures were maintained in the soil profile around the ATS up to 1 m above the initial permafrost table for four consecutive years (up to September 2022). Similar results can be expected for the STS, but after annual frozen ground becomes regenerated. Considering the snow cones generated frozen ground within two years of operation, with a much lower degree of net annual cooling (Table 3), it is likely the STS would generate frozen ground following an additional winter of operation.

5.2. Effects of snow reduction

Snow is a critically important cryogenic element of northern environments (Mellander et al., 2007) whose effect on subsurface thermal regimes varies with its depth, density, structure and duration on the ground (Zhang, 2005). Although the STS and ATS sites experienced greater ground cooling than the snow reduction cones, analysis of the data from below the latter indicates that such instruments, even when unaccompanied by thermosiphons, can alter the annual thermal regime of the soil from net positive (warming) to net negative (cooling). For this study, such cooling included the development of year-round sub-zero ground temperatures in the 0.7 to 0.8 m depth range within two years of installation.

This study quantifies the effect of snow cover reduction on ground thermal regimes and demonstrates that a simple instrument designed to reduce snow cover offers a practical and inexpensive solution for cases where a minimal decrease in subsurface temperature is sufficient to preserve permafrost. Since the West Cone was found to increase heat

Table 4
Summary of net annual heat transfer calculated from September 1 to August 31 of each year estimated ~0.25–1.00 m below ground for the controls and thermosiphons and 0.25–0.8 m for the snow cones.

Site	System	Net Annual Heat Transfer (W)					
		2018–2019	±	2019–2020	±	2020–2021	±
West Site	West Control	507	16	442	10	405	9
	West Cone	−173	9	–	–	–	–
	Active TS	−811	75	−1165	96	−979	88
East Site	East Control	–	–	98	3	263	10
	East Cone	−187	13	−657	42	−354	28
	Passive TS	–	–	−449	18	–	–

The uncertainty (±) is the average difference in heat transfer calculated using the upper and lower values of porosity. A negative or positive value indicates a net heat loss or gain, respectively.

Table 5
Summary of seasonal heat transfer (2019–2020) estimated ~0.25–1.00 m below ground for the controls and thermosiphons and the top 0.8 m for the cones.

Site	System	Seasonal Heat Transfer (W)							
		Fall 2019	±	Winter 2019–2020	±	Spring 2020	±	Summer 2020	±
West Site	West Control	−44	3	−175	8	460	19	201	3
	West Cone	2	1	−464	24	–	–	–	–
	Advanced TS	−242	21	−1156	87	0	1	233	13
East Site	East Control	28	1	−179	7	6	0	243	9
	East Cone	101	2	−997	26	−115	3	313	7
	Simple TS	−86	9	−829	61	88	5	378	18

The uncertainty (±) is the average difference in heat transfer calculated using the upper and lower values of porosity. A negative or positive value indicates a net heat loss or gain, respectively. Fall: September 1 to November 30, Winter: December 1 to March 31, Spring: April 1 to June 30, Summer: July 1 to August 31.

transfer from the ground by 10–18% compared to the West Control, it is suggested that including a snow cone in the design of the ATS (Fig. 3b) increased overall ground cooling proportionately. The cone may also reduce the thaw rate during the snow-free period by providing shade to the ground surface and by reflecting solar radiation, thought evidence for this shading effect is minimal in the seasonal heat flux calculations presented in Table 5.

A snow reduction cone added to a thermosiphon can therefore significantly increase the impact on ground cooling. Numerous snow reduction methods have been used to promote ground cooling, particularly along transportation corridors such as on the Baikal-Amur Mainline, Russia (e.g., Kondratiev, 2013), the Qinghai-Tibet Highway, China (e.g., Niu et al., 2008), or the Alaska Highway, Canada (Gagnon et al., 2022). The present study supports this work, demonstrating the benefits of incorporating snow reduction into the design of a thermosiphon specifically for wetlands, a dominant terrain type of subarctic regions that is not well represented by data from transportation corridors.

5.3. Effects of soil moisture on heat transfer estimates

The heat transfer calculations provide a first approximation of the heat removed by the ground cooling systems presented in this study as compared to similar control sites. The heat transfer calculations were most influenced by moisture conditions near-surface (dry or saturated in this case) and less sensitive to porosity (Table S1). Since near-surface peat has porosities from 79 to 94%, the addition of even a thin (10–20 cm) unsaturated zone was sufficient to impede vertical heat transfer (results not presented) despite the depth-weighted averaging approach for estimating thermal conductivity. The time of year when the unsaturated zone was present also influenced the annual energy balance. For example, net annual cooling was only achieved for the West Cone when an unsaturated zone was included to offset summer heating, but winter conditions remained saturated. Since frozen ground was being generated below the West Cone (physically measured), it suggested net cooling had to be occurring and supported the inclusion of a summer unsaturated zone in the analysis. Additionally, the thermal insulation from unsaturated peat in summer and enhanced heat removal from saturated frozen peat in winter is commonly attributed to permafrost protection in subarctic peatlands (e.g., Brown, 1963; Camill, 1999; Quinton and Baltzer, 2013; Woo, 2012).

In the absence of moisture content and water level data for the period of analysis, a simplified approach was undertaken to compare the performance of each ground cooling system. The effect of near-surface moisture conditions on the heat transfer results suggests future research should incorporate more robust temporal moisture content measurements into the analysis to refine these estimates. Such measurements will also be important when evaluating ground cooling systems under future climate change scenarios as air temperatures increase and precipitation patterns change (Bring et al., 2017; Derksen et al., 2015; Larsen et al., 2014; Liston and Hiemstra, 2011).

5.4. System advantages and limitations

All three systems assessed in this study are relatively low-cost and easily deployable compared to the industry alternatives. Comparing the performance of the systems in this study to commercially available systems is challenging considering subsurface and environmental conditions will greatly impact heat transfer rates (Zarling et al., 1990). However, it is anticipated that the thermosiphons assessed in this study would be less efficient than two-phased thermosiphons common in industry due to the importance of using a low viscosity working fluid for heat transfer efficiency (Long and Zarling, 2004).

While comparing the cost of a single-phase and two-phase thermosiphons without specific project details is challenging, certain advantages of a single-phase thermosiphons are apparent. The main distinction lies in the absence of compressed gas in a single-phase thermosiphon, resulting in potential cost advantages. Additionally, installation of a single-phase thermosiphon requires less qualified labor (required for installation of high-pressure components) compared to two-phase systems. An approximate cost for a single-phase thermosiphon range is a few hundred dollars compared to a few thousand dollars for a two-phase thermosiphon. Single-phase design not only offers an easily deployable, cost-effective alternative for small scale projects and private infrastructure support, but it is also compatible with an existing pile foundation technology, which means that incorporating single-phase thermosiphons into existing pile foundations can be achieved without requiring significant structural changes, making one-phase thermosiphons a cost-effective solution as an add-on component for existing ground cooling systems.

The low-cost single-phase TS designs, particularly in combination with snow reduction component, offer the ability to generate and maintain frozen ground in ground conditions that are highly saturated and relatively warm. Given their performance in these systems with high thermal inertia, it is expected that they would perform just as well or better in unsaturated mineral soils, and the differences in performance between the systems would be similar.

When fully operational, the ATS system demonstrated the highest heat transfer, and although individual components (e.g., mechanical pump) can fail due to extreme weather conditions, natural convection maintained heat transfer even in the case of enhanced circulation shutdown. Although the thermosiphons have the potential to conduct heat into the ground through the stationary fluid during summer, this appears to be relatively minor and is compensated during winter to produce net annual cooling. From September 2019–2020, the net heat loss from the ground below the East Cone was almost half of that lost from around the STS (Table 3). This suggests that the addition of a snow reduction cone to the STS design would significantly enhance its performance, while remaining a low-maintenance and passive option. Two crucial factors must be considered when estimating the effectiveness of the thermosiphons: the minimum temperature to which the thermosiphon is exposed during winter, and the area of the thermosiphon that is exposed above the ground. While winter temperatures cannot be controlled, the effectiveness of a thermosiphon can be enhanced by

increasing its exposed area. Given that both thermosiphons were installed in peat with 80% porosity, and the water table was approximately at the ground surface, the performance of the thermosiphons was considered effective for the duration of their operation and are expected to freeze the taliks and maintain aggregated permafrost. Further research is required to explore the relationship between the area of the exposed part of the thermosiphon above the ground and the depth of effective ground cooling, involving on-site experiments and mathematical modelling.

All three systems have potential applications within and in proximity to remote communities, such as in support of local infrastructure, as well as relatively simple and affordable tools to support customised strategies to adapt to permafrost thaw.

6. Conclusions

This study compared three ground cooling systems including a passive single-phase thermosiphon (STS), a single-phase active thermosiphon with snow reduction cone (ATS), and a stand-alone snow reduction cone. It was demonstrated that all three systems can be used to reduce ground temperatures in a high saturation peat environment. The advanced design demonstrated the greatest net ground cooling. However, the simple design appeared to be as effective at cooling the ground as the ATS during its one winter of operation while having no energy dependency, making it less prone to failure. Stand-alone snow reduction cones maintained annual ground temperatures below 0 °C at 0.7–0.8 m depths and generated frozen ground that increased in thickness over the study period. Although snow reduction is a dominant factor, other processes such as shading from solar radiation, may have contributed to the overall ground cooling effect. Results from this study indicate that the addition of a snow reduction cone enhances the performance of thermosiphons. Thus, an STS equipped with the snow reduction cone presents an attractive alternative to the ATS design given its much lower cost, greater versatility and ease of deployment and use.

This study emphasizes the importance of identifying localized geophysical and environmental conditions as the basis for determining the most suitable cooling system for mitigation and control of ground thermal profiles. Although thermosiphon technology has been used to suit a range of applications for over 60 years and its purpose is well acknowledged, the alarming rate of climate change in the North emphasizes the importance of novel mitigation and adaptation strategies designed for a range of soil types. Considering the prospective applications of ground cooling technologies, the novel ground cooling systems must integrate performance and deployment efficiency, maintenance accessibility and cost considerations.

This investigation supports the development of low cost, readily deployable ground cooling devices that may serve to mitigate permafrost thaw and improve the adaptability of engineering designs to a wide range of changing environmental conditions.

Author statement

This Author Statement is to certify that all authors have seen and approved the final version of the manuscript being submitted. They warrant that the article is the authors' original work, hasn't received prior publication and isn't under consideration for publication elsewhere.

CRediT authorship contribution statement

Ela Mastej: Conceptualization, Data curation, Formal analysis, Investigation, Methodology, Validation, Writing – original draft, Writing – review & editing. **Stephanie Wright:** Conceptualization, Data curation, Formal analysis, Writing – review & editing. **Michael Braverman:** Conceptualization, Data curation, Formal analysis, Investigation, Methodology, Resources, Supervision, Writing – review & editing. **Élise Devoie:** Conceptualization, Data curation, Formal analysis, Software, Validation, Writing – review & editing. **Igor Egorov:** Conceptualization, Data curation, Formal analysis, Investigation, Methodology, Resources, Writing – review & editing. **William Quinton:** Conceptualization, Funding acquisition, Methodology, Project administration, Resources, Supervision, Writing – review & editing.

Declaration of Competing Interest

The authors declare that they have no known competing financial interests or personal relationships that could have appeared to influence the work reported in this paper.

Data availability

Data will be made available on request.

Acknowledgements

We would like to acknowledge that the Scotty Creek Research station is located on treaty 11 land. We wish to thank the Dehcho First Nations and Liidlii Kue First Nation for their support and partnership in conducting this research on their traditional lands. We also would like to thank acknowledge the Scotty Creek Research Station for hosting this research project. Special thanks to Mason Dominico for all his unwavering technical assistance, Caren Ackley, Dr. Kristine Haynes and Dr. Goeff Kershaw for their guidance and support and Dr. Jon Warland for his unparalleled insight into the integral fabric of science and humanity. A special recognition for the late Dr. Matti Seppälä for his pioneering work on snow insulation and palsa formation and deep gratitude for his support of this project.

This work was supported by ArcticNet-Dehcho Collaborative on Permafrost [DCoP-P02], NSERC Postdoctoral Fellowship [PDF-568264-2022; PDF-557503-2021], GHD Consulting and the National Research Council of Canada.

Appendix A. Supplementary data

Supplementary data to this article can be found online at https://doi.org/10.1016/j.coldregions.2023.104095.

References

Ahmed, Al Jubori, A.M., 2021. Assessment of heat transfer and flow characteristics of a two phase closed thermosiphon. Heat Transfer (Hoboken, N.J Print) 50 (2), 1351–1370.

Azizi, M., Hosseini, M., Zafarnak, S., Shanbedi, M., Amiri, A., 2013. Experimental analysis of thermal performance in a two-phase closed thermosiphon using graphene/water nanofluid. Ind. Eng. Chem. Res. 52 (29), 10015–10021.

Badache, M., Aidoun, Z., Eslami-Nejad, P., Blessent, D., 2019. Ground-coupled natural circulating devices (thermosiphons): a review of modeling, experimental and development studies. Inventions (Basel) 4 (1), 14–57.

Bring, A., Shiklomanov, A., Lammers, R.B., 2017. Pan-Arctic river discharge: Prioritizing monitoring of future climate change hot spots. Earth's Future 5, 72–92. https://doi.org/10.1002/2016EF000434.

Brown, R.J.E., 1963. Influence of vegetation on permafrost. In: Proceedings of the 9th International Conference on Permafrost. Presented at the Permafrost International Conference, Fairbanks, Alaska, pp. 125–130.

Brusly Solomon, A., Arul Daniel, V., Ramachandran, K., Pillai, B.C., Renjith Singh, R., Sharifpur, M., Meyer, J.P., 2017. Performance enhancement of a two-phase closed thermosiphon with a thin, porous copper coating. Int. Commun. Heat Mass Transf. 82, 9–19. https://doi.org/10.1016/j.icheatmasstransfer.2017.02.001.

Burgess, M.M., Smith, S.L., 2000. Shallow Ground Temperatures, the Physical Environment of the Mackenzie Valley, Northwest Territories: A Base Line for the Assessment of Environmental Change. Geological Survey of Canada.

Camill, P., 1999. Peat accumulation and succession following permafrost thaw in the boreal peatlands of Manitoba, Canada. Écoscience 6, 592–602. https://doi.org/10.1080/11956860.1999.11682561.

Carpino, O.A., Berg, A.A., Quinton, W.L., Adams, J.R., 2018. Climate change and permafrost thaw-induced boreal forest loss in northwestern Canada. Environ. Res. Lett. 13, 084018 https://doi.org/10.1088/1748-9326/aad74e.

Carpino, O., Haynes, K., Connon, R., Craig, J., Devoie, É., Quinton, W., 2021. Long-term climate-influenced land cover change in discontinuous permafrost peatland

complexes. Hydrol. Earth Syst. Sci. 25, 3301–3317. https://doi.org/10.5194/hess-25-3301-2021.
Chasmer, L., Hopkinson, C., 2017. Threshold loss of discontinuous permafrost and landscape evolution. Glob. Chang. Biol. 23, 2672–2686. https://doi.org/10.1111/gcb.13537.
Chen, L., Yu, W., Lu, Y., Liu, W., 2018. Numerical simulation on the performance of thermosyphon adopted to mitigate thaw settlement of embankment in sandy permafrost zone. Appl. Therm. Eng. 128, 1624–1633. https://doi.org/10.1016/j.applthermaleng.2017.09.130.
Cheng, G., Sun, Z., Niu, F., 2008. Application of the roadbed cooling approach in Qinghai–Tibet railway engineering. Cold Reg. Sci. Technol. 53, 241–258.
Cline, D.W., 1997. Effect of seasonality of snow accumulation and melt on snow surface energy exchanges at a continental alpine site. J. Appl. Meteorol. Climatol. 36, 32–51. https://doi.org/10.1175/1520-0450(1997)036<0032:EOSOSA>2.0.CO;2.
Cohen, J.L., 1994. Snow cover and climate. Weather 49, 150–156.
Connon, R.F., Quinton, W.L., Craig, J.R., Hayashi, M., 2014. Changing hydrologic connectivity due to permafrost thaw in the lower Liard River valley, NWT, Canada. Hydrol. Process. 28, 4163–4178. https://doi.org/10.1002/hyp.10206.
Connon, R.F., Quinton, W.L., Craig, J.R., Hanisch, J., Sonnentag, O., 2015. The hydrology of interconnected bog complexes in discontinuous permafrost terrains. Hydrol. Process. 29, 3831–3847. https://doi.org/10.1002/hyp.10604.
Connon, R., Devoie, É., Hayashi, M., Veness, T., Quinton, W., 2018. The influence of shallow taliks on permafrost thaw and active layer dynamics in subarctic Canada. J. Geophys. Res. Earth 123, 281–297. https://doi.org/10.1002/2017JF004469.
Davidson, D.J., Williamson, T., Parkins, J.R., 2003. Understanding climate change risk and vulnerability in northern forest-based communities. Can. J. For. Res. 33, 2252–2261. https://doi.org/10.1139/x03-138.
Derksen, C., Brown, R., Mudryk, L., Luojus, K., 2015. Terrestrial snow cover [in "State of the Climate in 2014"]. Bull. Amer. Meteor. Soc. 96 (7), S133–S135. https://doi.org/10.1175/2015BAMSStateoftheClimate.1.
Devoie, É.G., Craig, J.R., Connon, R.F., Quinton, W.L., 2019. Taliks: a tipping point in discontinuous permafrost degradation in peatlands. Water Resour. Res. 55, 9838–9857. https://doi.org/10.1029/2018WR024488.
Devoie, É.G., Craig, J.R., Dominico, M., Carpino, O., Connon, R.F., Rudy, A.C.A., Quinton, W.L., 2021. Mechanisms of discontinuous permafrost thaw in peatlands. J. Geophys. Res. Earth 126. https://doi.org/10.1029/2021JF006204 e2021JF006204.
Doré, G., Niu, F., Brooks, H., 2016. Adaptation methods for transportation infrastructure built on degrading permafrost. Permafr. Periglac. Process. 27 (4), 352–364. https://doi.org/10.1002/ppp.1919.
Edlund, J., Gordon, G., & Robinson, P. (1998). A model mine shows its cracks. *Unpublished report by Pacific Environment. http://pacificenvironment.org/downloads/model_mine*.
Environment and Climate Change Canada, 2021. Climate Change and Variations Bulletin. Government of Canada. https://www.canada.ca/en/environment-climate-change/services/climate-change/science-research-data/climate-trends-variability/trends-variations.html.
Esch, D., 1988. Embankment case histories on permafrost. In: Johnson, E.G. (Ed.), Embankment Design and Construction in Cold Regions: an ASCE Monograph. American Society of Civil Engineers, New York, New York, USA, pp. 127–159.
Faria, D.A., Pomeroy, J.W., Essery, R.L.H., 2000. Effect of covariance between ablation and snow water equivalent on depletion of snow-covered area in a forest. Hydrol. Process. 14, 2683–2695.
Forsstrom, A.M., Long, E.L., Zarling, J.P., Knutsson, S., 2002. Thermosyphon cooling of Chena Hot Springs Road test section. In: Proceedings of the 11th International Conference in Cold Regions Engineering. ASCE, Anchorage, AK, pp. 645–655.
Gagnon, Fortier, D., Sliger, M., Rioux, K., 2022. Air-convection-reflective sheds: a mitigation technique that stopped degradation and promoted permafrost recovery under the Alaska Highway, South-Western Yukon, Canada. Cold Reg. Sci. Technol. 197 https://doi.org/10.1016/j.coldregions.2022.103524, 103524.
Garon-Labrecque, M.-È., Léveillé-Bourret, É., Higgins, K., Sonnentag, O., 2015. Additions to the boreal flora of the Northwest Territories with a preliminary vascular flora of Scotty Creek. Canad. Field-Nat. 129, 349–367. https://doi.org/10.22621/cfn.v129i4.1757.
GNWT, 2018. Northern Voices, Northern Waters: NWT Water Stewardship Strategy. Government of the Northwest Territories, Yellowknife, NT.
Goetz, P., 2010. Preserving Arctic Archaeology in the 21st Century: Threats of Climate Change (Masters Thesis). University of Waterloo, Waterloo, Canada.
Hayashi, M., Goeller, N., Quinton, W.L., Wright, N., 2007. simple heat-conduction method for simulating the frost-table depth in hydrological models. Hydrol. Processes 21 (19), 2610–2622. https://doi.org/10.1002/hyp.6792.
Hayley, D.W., Roggensack, W.D., Jubien, W.E., Johnson, P.V., 1983. Stabilization of sinkholes on the Hudson Bay railway. In: Proceedings of the 4th International Conference on Permafrost. National Academy Press, pp. 468–472.
Hayley, D., Seto, J., Grapel, C., Cathro, D., Valeriote, M., 2004. Performance of two rockfill dams with thermosyphons on permafrost foundations, Ekati Diamond Mine, NT. In: Presented at the 57th Canadian Geotechnical Conference, Quebec City.
Haynes, K.M., Connon, R.F., Quinton, W.L., 2019. Hydrometeorological measurements in peatland-dominated, discontinuous permafrost at Scotty Creek, Northwest Territories, Canada. Geosci. Data J 6 (2), 85–96. https://doi.org/10.1002/gdj3.69.
He, H., Dyck, M.F., Si, B.C., Zhang, T., Lv, J., Wang, J., 2015. Soil freezing–thawing characteristics and snowmelt infiltration in Cryalfs of Alberta, Canada. Geoderma Reg. 5, 198–208. https://doi.org/10.1016/j.geodrs.2015.08.001.
Heuer, C.E., 1979. The Application of Heat Pipes on the Trans-Alaska Pipeline. Directorate of Military Programs Office, Chief of Engineers. US Army Cold Regions Research and Engineering Laboratory, Hanover, NH.
Jaeger, J.C., Carslaw, H.S., 1959. Conduction of Heat in Solids. Clarendon Press, United Kingdom.
Jafarov, E.E., Coon, E.T., Harp, D.R., Wilson, C.J., Painter, S.L., Atchley, A.L., Romanovsky, V.E., 2018. Modeling the role of preferential snow accumulation in through talik development and hillslope groundwater flow in a transitional permafrost landscape. Environ. Res. Lett. 13, 105006 https://doi.org/10.1088/1748-9326/aadd30.
Kim, Moon, J.H., 2021. Numerical investigation and modeling of thermal resistance and effective thermal conductivity for two-phase thermosyphon. Case Stud. Therm. Eng. 27, 101358. https://doi.org/10.1016/j.csite.2021.101358.
Kondratiev, V.G., 2013. Geocryological problems of railroads on permafrost. In: ISCORD 2013: Planning for Sustainable Cold Regions, pp. 191–203.
Larsen, J.N., Anisimov, O.A., Constable, A., Hollowed, A.B., Maynard, N., Prestrud, P., Prowse, T.D., Stone, J.M.R., 2014. Polar regions. In: Barros, V.R., et al. (Eds.), Climate Change 2014: Impacts, Adaptation, and Vulnerability. Part B: Regional Aspects. Cambridge University Press, pp. 1567–1612.
Lienhard IV, J.H., Lienhard V, J.H., 2006. A Heat Transfer Textbook, 3rd ed. Phlogiston Press, Cambridge, MA.
Liston, G.E., Hiemstra, C.A., 2011. The changing cryosphere: Pan-Arctic snow trends (1979–2009). J. Clim. 24, 5691–5712. https://doi.org/10.1175/JCLI-D-11-00081.1.
Long, E.L., Zarling, J.P., 2004. Passive Techniques for Ground Temperature Control, pp. 77–165. https://doi.org/10.1061/9780784407202.ch04.
Malenfant-Lepage, J., Doré, G., Fortier, D., 2012a. Thermal effectiveness of the mitigation techniques tested at Beaver Creek Experimental Road Site based on a heat balance analysis (Yukon, Canada). In: Morse, B., Doré, G. (Eds.), Cold Regions 2012: Sustainable Infrastructure Development in a Changing Cold Environment, 19–22 August, Quebec City, Quebec, Canada. American Society of Civil Engineers, Reston, Virginia, USA, pp. 42–51. https://doi.org/10.1061/9780784412473.005.
Malenfant-Lepage, J., Doré, G., Fortier, D., Murchison, P., 2012b. Thermal performance of the permafrost protection techniques at Beaver Creek Experimental Road Site, Yukon, Canada. In: Extended Abstracts of the10th International Conference on Permafrost, 25–29 June, Salekhard, Russia. The Northern Publisher, Salekhard, Russia, pp. 261–266.
Marshall, S., Oglesby, R.J., Nolin, A.W., 2003. The Predictability of Winter Snow Cover over the Western United States. J. Clim. 16, 1062–1073. https://doi.org/10.1175/1520-0442(2003)016<1062:TPOWSC>2.0.CO;2.
McClymont, A.F., Hayashi, M., Bentley, L.R., Christensen, B.S., 2013. Geophysical imaging and thermal modeling of subsurface morphology and thaw evolution of discontinuous permafrost. J. Geophys. Res. Earth 118, 1826–1837. https://doi.org/10.1002/jgrf.20114.
McFadden, T., 1985. Performance of the Thermotube Permafrost Stabilization System in the Airport Runway at Bethel, Alaska. AK Department of Transportation.
Mellander, P.-E., Löfvenius, M.O., Laudon, H., 2007. Climate change impact on snow and soil temperature in boreal Scots pine stands. Clim. Chang. 85, 179–193. https://doi.org/10.1007/s10584-007-9254-3.
Niu, F., Xu, J., Lin, Z., Wu, Q., Cheng, G., 2008. Permafrost characteristics of the Qinghai-Tibet Plateau and methods of roadbed construction of railway. Acta Geol. Sin. Engl. Ed. 82 (5), 949–958. https://doi.org/10.1111/j.1755-6724.2008.tb00650.x.
Niu, F.J., Ge, J.J., Feng, W.J., Liu, H., 2010. Engineering effects of sunshine-shield roadbed of the Qinghai-Tibet Railway in permafrost region. J. Glaciol. Geocryol. 32, 325–334.
O'Neill, H.B., Burn, C.R., 2017. Impacts of variations in snow cover on permafrost stability, including simulated snow management, Dempster Highway, Peel Plateau, Northwest Territories. Arctic Sci. 3, 150–178. https://doi.org/10.1139/as-2016-0036.
Pei, W., Zhang, M., Lai, Y., Yan, Z., Li, S., 2019. Evaluation of the ground heat control capacity of a novel air-L-shaped TPCT-ground (ALTG) cooling system in cold regions. Energy 179 (Complete), 655–668.
Pomeroy, J.W., Gray, D.M., Brown, T., Hedstrom, N.R., Quinton, W.L., Granger, R.J., Carey, S.K., 2007. The cold regions hydrological process representation and model: a platform for basing model structure on physical evidence. Hydrol. Process. 21 (19), 2650–2667.
Quinton, W.L., Baltzer, J.L., 2013. The active-layer hydrology of a peat plateau with thawing permafrost (Scotty Creek, Canada). Hydrogeol. J. 21, 201–220. https://doi.org/10.1007/s10040-012-0935-2.
Quinton, W.L., Hayashi, M., Carey, S.K., 2008. Peat hydraulic conductivity in cold regions and its relation to pore size and geometry. Hydrol. Process. 22, 2829–2837. https://doi.org/10.1002/hyp.7027.
Quinton, W.L., Hayashi, M., Chasmer, L.E., 2009. Peatland hydrology of discontinuous permafrost in the northwest territories: overview and synthesis. Can. Water Resour. J. 34, 311–328. https://doi.org/10.4296/cwrj3404311.
Quinton, W.L., Hayashi, M., Chasmer, L.E., 2011. Permafrost-thaw-induced land-cover change in the Canadian subarctic: implications for water resources. Hydrol. Process. 25, 152–158. https://doi.org/10.1002/hyp.7894.
Quinton, W., Berg, A., Braverman, M., Carpino, O., Chasmer, L., Connon, R., Craig, J., Devoie, É., Hayashi, M., Haynes, K., Olefeldt, D., Pietroniro, A., Rezanezhad, F., Schincariol, R., Sonnentag, O., 2019. A synthesis of three decades of hydrological research at Scotty Creek, NWT, Canada. Hydrol. Earth Syst. Sci. 23, 2015–2039. https://doi.org/10.5194/hess-23-2015-2019.
Rahman, M.A., Saghir, M.Z., 2014. Thermodiffusion or soret effect: historical review. Int. J. Heat Mass Transf. 73, 693–705. https://doi.org/10.1016/j.ijheatmasstransfer.2014.02.057.
Raynolds, M.K., Walker, D.A., Ambrosius, K.J., Brown, J., Everett, K.R., Kanevskiy, M., Kofinas, G.P., Romanovsky, V.E., Shur, Y., Webber, P.J., 2014. Cumulative geoecological effects of 62 years of infrastructure and climate change in ice-rich

permafrost landscapes, Prudhoe Bay Oilfield, Alaska. Glob. Chang. Biol. 20, 1211–1224. https://doi.org/10.1111/gcb.12500.
Richardson, P., 1979. Tough Alaska conditions prove new pile design's versatility. Alaska Constr. Oil. February: 20–28.
Richter-Menge, J., Jeffries, M.O., Osborne, E., 2017. State of the climate in 2017. The Arctic 99, 143–173.
Smith, S.L., Romanovsky, V.E., Lewkowicz, A.G., Burn, C.R., Allard, M., Clow, G.D., Yoshikawa, K., Throop, J., 2010. Thermal state of permafrost in North America: a contribution to the international polar year. Permafr. Periglac. Process. 21, 117–135. https://doi.org/10.1002/ppp.690.
St. Jacques, J.-M., Sauchyn, D.J., 2009. Increasing winter baseflow and mean annual streamflow from possible permafrost thawing in the Northwest Territories, Canada. Geophys. Res. Lett. 36 https://doi.org/10.1029/2008GL035822.
Vincent, L.A., Zhang, X., Brown, R.D., Feng, Y., Mekis, E., Milewska, E.J., Wan, H., Wang, X.L., 2015. Observed trends in Canada's climate and influence of low-frequency variability modes. J. Clim. 28, 4545–4560. https://doi.org/10.1175/JCLI-D-14-00697.1.
Wagner, A.M., 2014. Review of Thermosyphon Applications. US Army Corps of Engineers, Cold Regions Research and Engineering Laboratory. ERDC/CRREL TR-14-1.
Wenjie, F., Wei, M., Dongqing, L., Luxin, Z., 2006. Application investigation of awning to roadway engineering on the Qinghai-Tibet Plateau. Cold Reg. Sci. Technol. 45 (1), 51–58. https://doi.org/10.1016/j.coldregions.2006.01.004.
Williams, T.J., Quinton, W.L., Baltzer, J.L., 2013. Linear disturbances on discontinuous permafrost: implications for thaw-induced changes to land cover and drainage patterns. Environ. Res. Lett. 8, 025006 https://doi.org/10.1088/1748-9326/8/2/025006.
Woo, M., 2012. Permafrost Hydrology. Springer-Verlag, Berlin Heidelberg. https://doi.org/10.1007/978-3-642-23462-0.
Wright, S.N., Thompson, L.M., Olefeldt, D., Connon, R.F., Carpino, O.A., Beel, C.R., Quinton, W.L., 2022. Thaw-induced impacts on land and water in discontinuous permafrost: a review of the Taiga Plains and Taiga Shield, northwestern Canada. Earth Sci. Rev. 232, 104104 https://doi.org/10.1016/j.earscirev.2022.104104.
Wu, J., Ma, W., Sun, Z., Wen, Z., 2010. In-situ study on cooling effect of the two-phase closed thermosyphon and insulation combinational embankment of the Qinghai Tibet Railway. Cold Reg. Sci. Technol. 60, 234–244.
Xu, J., Goering, D.J., 2008. Experimental validation of passive permafrost cooling systems. Cold Regions Science and Technology 53 (3), 283–297.
Zarling, J.P., & Braley, W.A. (1986). *Thaw Stabilization of Roadway Embankments Constructed over Permafrost. DRAFT FINAL REPORT* (No. FHWA-AK-87-20).
Zarling, J., Brayley, W., 1987. Thaw Stabilization of Roadway Embankments Constructed over Permafrost. Fairbanks, AK.
Zarling, J.P., Hansen, P., Kozisek, L., 1990. Design and performance experience of foundations stabilized with thermosyphons. In: Permafrost Canada: Proceedings of the Fifth Canadian Permafrost Conference. Quebec, Centre d'études nordiques, l'Université Laval, Canada.
Zhang, T., 2005. Influence of the seasonal snow cover on the ground thermal regime: an overview. Rev. Geophys. 43 https://doi.org/10.1029/2004RG000157.
Zhang, B., Sheng, Y., Chen, J., Li, J., 2011. In-situ test study on the cooling effect of two-phase closed thermosyphon in marshy permafrost regions along the Chaidaer–Muli Railway, Qinghai Province, China. Cold Reg. Sci. Technol. 65, 456–464.
Zhang, F., Zhang, H., Hagen, S.C., Ye, M., Wang, D., Gui, D., Zeng, C., Tian, L., Liu, J., 2015. Snow cover and runoff modelling in a high mountain catchment with scarce data: effects of temperature and precipitation parameters. Hydrol. Process. 29, 52–65. https://doi.org/10.1002/hyp.10125.
Zhang, Lai, Y., Wu, Q., Yu, Q., Zhao, T., Pei, W., Zhang, J., 2016. A full-scale field experiment to evaluate the cooling performance of a novel composite embankment in permafrost regions. Int. J. Heat Mass Transf. 95, 1047–1056.
Zhi, W., Yu, S., Wei, M., Jilin, Q., Wu, J., 2005. Analysis on effect of permafrost protection by two-phase closed thermosyphon and insulation jointly in permafrost regions. Cold Reg. Sci. Technol. 43, 150–163. https://doi.org/10.1016/j.coldregions.2005.04.001.
Zoltai, S.C., Tarnocai, C., 1974. Perennially frozen peatlands in the western arctic and subarctic of Canada. Can. J. Earth Sci. https://doi.org/10.1139/e75-004.